



OPEN

Alkyl chain length of quaternized SBA-15 and solution conditions determine hydrophobic and electrostatic interactions for carbamazepine adsorption

Jin-Kyu Kang¹, Hyebin Lee², Song-Bae Kim³ & Hyokwan Bae^{2,4}✉

Santa Barbara Amorphous-15 (SBA) is a stable and mesoporous silica material. Quaternized SBA-15 with alkyl chains (Q_{SBA}) exhibits electrostatic attraction for anionic molecules via the N^+ moiety of the ammonium group, whereas its alkyl chain length determines its hydrophobic interactions. In this study, Q_{SBA} with different alkyl chain lengths were synthesized using the trimethyl, dimethyloctyl, and dimethyloctadecyl groups ($C1Q_{SBA}$, $C8Q_{SBA}$, and $C18Q_{SBA}$, respectively). Carbamazepine (CBZ) is a widely prescribed pharmaceutical compound, but is difficult to remove using conventional water treatments. The CBZ adsorption characteristics of Q_{SBA} were examined to determine its adsorption mechanism by changing the alkyl chain length and solution conditions (pH and ionic strength). A longer alkyl chain resulted in slower adsorption (up to 120 min), while the amount of CBZ adsorbed was higher for longer alkyl chains per unit mass of Q_{SBA} at equilibrium. The maximum adsorption capacities of $C1Q_{SBA}$, $C8Q_{SBA}$, and $C18Q_{SBA}$ were 3.14, 6.56, and 24.5 mg/g, respectively, as obtained using the Langmuir model. For the tested initial CBZ concentrations (2–100 mg/L), the adsorption capacity increased with increasing alkyl chain length. Because CBZ does not dissociate readily ($pK_a = 13.9$), stable hydrophobic adsorption was observed despite the changes in pH (0.41–0.92, 1.70–2.24, and 7.56–9.10 mg/g for $C1Q_{SBA}$, $C8Q_{SBA}$, and $C18Q_{SBA}$, respectively); the exception was pH 2. Increasing the ionic strength from 0.1 to 100 mM enhanced the adsorption capacity of $C18Q_{SBA}$ from 9.27 ± 0.42 to 14.94 ± 0.17 mg/g because the hydrophobic interactions were increased while the electrostatic attraction of the N^+ was reduced. Thus, the ionic strength was a stronger control factor determining hydrophobic adsorption of CBZ than the solution pH. Based on the changes in hydrophobicity, which depends on the alkyl chain length, it was possible to enhance CBZ adsorption and investigate the adsorption mechanism in detail. Thus, this study aids the development of adsorbents suitable for pharmaceuticals with controlling molecular structure of Q_{SBA} and solution conditions.

The ever-increasing production, consumption, and release into environment of pharmaceutical and personal care products (PPCPs) has become a global concern^{1,2}. Carbamazepine (CBZ) is one of the four most widely prescribed pharmaceuticals for the treatment of epilepsy and psychosis^{3,4}. The extensive use and long durability/low degradability of CBZ have resulted in its detection in sewage, surface water, groundwater, and drinking water^{4,5}. CBZ cannot be treated adequately using conventional water treatments. Therefore, research efforts are underway to remove CBZ from the aqueous phase using advanced methods, such as filtration^{6–8}, biological processes⁹, advanced oxidation methods^{5,8–12}, coagulation/flocculation/sedimentation^{13,14}, and adsorption^{3,14–20}.

¹Institute for Environment and Energy, Pusan National University, 2 Busandaehak-ro 63beon-gil, Geumjeong-gu, Busan 46241, Republic of Korea. ²Graduate School of Carbon Neutrality, Ulsan National Institute of Science and Technology (UNIST), 50 UNIST-gil, Eonyang-eup, Ulju-gun, Ulsan 44919, Republic of Korea. ³Environmental Functional Materials and Water Treatment Laboratory, Department of Rural Systems Engineering, Seoul National University, 1 Kwanak-ro, Kwanak-gu, Seoul 08826, Republic of Korea. ⁴Department of Urban and Environmental Engineering, Ulsan National Institute of Science and Technology (UNIST), 50 UNIST-gil, Eonyang-eup, Ulju-gun, Ulsan 44919, Republic of Korea. ✉email: hyokwan.bae@unist.ac.kr

Among the various methods being explored, adsorption is particularly attractive because it is simple in design, easy to perform, cost-effective, and free of byproducts^{15,16}.

Since carbon-based materials (CBMs) have high specific surface areas and hydrophobic characteristics, they are being explored for use in various fields^{21–23}. They have also been studied widely for use as adsorbents with high sorption capacities for organic compounds^{24–28}. Zhu et al.²⁹ reported that the octanol/water distribution coefficient with respect to dissociation at pH 7 is proportional to the adsorption performance of the porous adsorbent or CBM used. They suggested that hydrophobic or π – π interactions are the major mechanisms of PPCP adsorption. Thus, the hydrophobic interactions between the PPCP in question and the adsorbent used have a determining effect on the adsorption process. The pK_a of an organic molecule determines the specific pH at which protonation or deprotonation occurs. Hence, PPCPs deprotonate and form negative ions at $pH < pK_a$, which inhibits the hydrophobic interactions between the CBM used and the PPCP^{30,31}. In addition, the ionic strength of the aqueous phase also affects the hydrophilic and hydrophobic interactions³². Therefore, the adsorption efficiency of CBZ, which is a representative persistent PPCP and does not readily undergo biological and physicochemical degradation^{33,34}, can be controlled based on the hydrophobicity of the adsorbent used and the environmental conditions such as pH and ionic strength.

Santa Barbara Amorphous-15 (SBA) is a stable and mesoporous silica material. The effects of the length of the alkyl chain attached to quaternized SBA-15 (Q_{SBA}) on its hydrophobic and hydrophilic adsorption properties have been studied^{35,36}. For example, Q_{SBA} with a long alkyl chain shows high adsorption for diclofenac (DCF) owing to both the hydrophobic interactions of the long alkyl chain and the electrostatic attraction of the N^+ species³⁶. For the nitrate ion, electrostatic adsorption on the N^+ species of the quaternary ammonium occurs readily even in the presence of competing oxyanions, such as bicarbonate, phosphate, and sulfate ions. This is owing to the high nitrate selectivity of Q_{SBA} because of its long-alkyl-chain-based hydrophobicity from higher hydration energy of nitrate than one of the other oxyanions³⁵. By controlling the hydrophobicity based on the length of the alkyl chain, the adsorption capacity and selectivity for the target contaminants can be improved, and the adsorption mechanism can be elucidated^{35,36}. However, in previous studies, the adsorption characteristics have been investigated only with respect to PPCPs based on different functional groups^{37,38}, and there has been no research on the adsorption characteristics of Q_{SBA} for PPCPs based on its hydrophobicity; the exception is DCF³⁶. CBZ has a lower hydrophobicity than DCF but does not dissociate under general pH conditions because of its high pK_a ^{39–42}. Therefore, its adsorption on Q_{SBA} is expected to be different from that of DCF in terms of the adsorption capacity, which would depend on the alkyl chain length. The results obtained for CBZ can be utilized to propose an appropriate alkyl chain length for Q_{SBA} in removing various PPCPs, considering their characteristics.

In this study, we examined the effects of the hydrophobicity of Q_{SBA} on CBZ adsorption by varying the alkyl chain length of Q_{SBA} as well as the aqueous conditions via batch experiments. The equilibrium adsorption capacity was evaluated by testing the effects of the initial CBZ concentration on its adsorption on Q_{SBA} with alkyl chains of different lengths (trimethyl, dimethyloctyl, and dimethyloctadecyl, which resulted in $C1Q_{SBA}$, $C8Q_{SBA}$, and $C18Q_{SBA}$, respectively). It was hypothesized that the changes in the hydrophobicity of Q_{SBA} would result in variations in the kinetics and equilibrium adsorption characteristics for hydrophobic CBZ. The pH and ionic strength of the test solution were also varied. This study provides additional insights into the molecular structure of Q_{SBA} for CBZ adsorption as well as the optimal characteristics of wastewater for the removal of CBZ.

Materials and methods

Quaternized SBA-15. $C1Q_{SBA}$, $C8Q_{SBA}$, and $C18Q_{SBA}$ were prepared using a previously reported method³⁵. Briefly, $C1Q_{SBA}$ was prepared according to the following procedure: 0.1 mol of trimethyl[3-(trimethoxysilyl)propyl]ammonium chloride (50% in methanol, Tokyo Chemical Industry, Tokyo, Japan) and 6 g of SBA (Sigma Aldrich, MO, USA) were stirred for 1 h in 100 mL of toluene (99.5%, Daejung, Siheung, Republic of Korea). The mixture was then refluxed with 1 mL of deionized (DI) water at 100 °C for 48 h. Next, the slurry was treated with 0.1 M NaCl, separated using a 0.45- μ m polyvinylidene fluoride (PVDF) filter, and dried at 65 °C in a drying oven until use. $C8Q_{SBA}$ and $C18Q_{SBA}$ were also prepared using the same processes as that employed for $C1Q_{SBA}$; the difference was that dimethyloctyl[3-(trimethoxysilyl)propyl]ammonium chloride and dimethyloctadecyl[3-(trimethoxysilyl)propyl]ammonium chloride (42% in methanol, Sigma Aldrich, MO, USA), respectively, were used instead of trimethyl[3-(trimethoxysilyl)propyl]ammonium chloride. Dimethyloctyl [3-(trimethoxysilyl)propyl]ammonium chloride was synthesized by reacting 0.1 mol of (3-chloropropyl)trimethoxysilane ($\geq 97\%$, Sigma Aldrich, MO, USA) and 0.1 mol of N,N-dimethyloctylamine (95%, Sigma Aldrich, MO, USA) at 85 °C for 48 h.

Test solution of CBZ. A 100 mg/L CBZ stock solution was prepared by dissolving 50 mg of CBZ ($\geq 98\%$, Sigma Aldrich) in 10 mL of methanol and then diluting it to 500 mL with DI water. There was no shift in the λ_{max} value (285 nm) of CBZ with the pH (Fig. S1). Therefore, the calibration curves of CBZ were obtained by measuring the absorbance of a serially diluted solution at 285 nm using an ultraviolet–visible spectrophotometer (Optizen POP, Mecasys, Korea) and 1-cm quartz cells for each pH.

Batch experiments. Because CBZ has high hydrophobicity and low solubility in water, it is difficult to test a wide range of concentrations in aqueous solutions. Furthermore, the dissociation of molecules greatly influences their solubility. Therefore, in this study, we examined the solubility to determine the concentration range for dissociation based on Eq. (1)³⁹:

$$S_H = S_0 \left(1 + \frac{K_a}{[H^+]} \right) \quad (1)$$

where S_H is the solubility in water at a specific pH (mg/L), and S_0 is the intrinsic solubility of an undissociated molecule. Because the pK_a of CBZ is very high (13.9), CBZ remains intact with low solubility at $pH < 13.9$. Therefore, the batch experiments to confirm its adsorption were conducted at concentrations of 100 mg/L or less, as S_0 is in the range of 112–236 mg/L.

Batch experiments were also performed for Q_{SBA} by varying the contact time, initial CBZ concentration, pH, and ionic strength. All these experiments were performed using 0.03 g of either C1 Q_{SBA} , C8 Q_{SBA} , or C18 Q_{SBA} . A 30 mL of the CBZ solution was poured into a 50-mL conical tube and incubated at 150 rpm and 25 °C in a shaking incubator. For each batch condition, the experiments were conducted in duplicate. After the reaction, the Q_{SBA} and solution were separated using a 0.45- μ m PVDF filter. The CBZ concentrations before and after the batch experiment were calculated using a calibration curve.

The reaction times, CBZ concentrations, pH, and ionic strengths are listed in Table S1, which also lists the reaction conditions. The reaction time was varied from 5 to 360 min at a fixed CBZ concentration of 40 mg/L. In the other experiments, the CBZ solution and Q_{SBA} were allowed to react for 24 h. The equilibrium adsorption capacity was measured for various initial concentrations of CBZ (2–100 mg/L). The effect of the pH was assessed by adjusting the initial pH of the CBZ solution (40 mg/L) to 2, 4, 6, 8, and 10 using 0.1 M HCl and 0.1 M NaOH. The effect of the ionic strength was evaluated by adding 0.1–100 mM NaCl to the CBZ solution (40 mg/L).

Data analysis. The amount of CBZ adsorbed during the reaction time (q_t) experiments was determined by fitting the data using various kinetic models (pseudo-first-order⁴³, pseudo-second-order⁴⁴, and Elovich⁴⁵ models, Table S1), while the amount of CBZ adsorbed at equilibrium (q_e) during the initial concentration experiments was fitted using the Freundlich⁴⁶, Langmuir⁴⁷, and Redlich–Peterson⁴⁸ models (Table S2). The optimal parameters for each model for each Q_{SBA} were obtained via nonlinear regression using the solver function in Excel 2019 (Microsoft Corporation, WA, USA). The coefficient of determination (Eq. 2) and sum of the squared error (Eq. 3) were used as the error functions for model comparison.

$$R^2 = \frac{\sum_{i=1}^m (y_c - \bar{y}_e)_i^2}{\sum_{i=1}^m (y_c - \bar{y}_e)_i^2 + \sum_{i=1}^m (y_c - y_e)_i^2} \quad (2)$$

$$SSE = \sum_{i=1}^n (y_e - y_c)_i^2 \quad (3)$$

where R^2 , Coefficient of determination; SSE , Sum of the squared error; y_c , Adsorption capacity calculated using the model; y_e , Adsorption capacity measured experimentally; \bar{y}_e , Average measured adsorption capacity.

Characteristics of quaternized SBA-15 and CBZ. Figure 1 shows a schematic of the procedure for preparing the Q_{SBA} samples and digital images of the samples. X-ray photoelectron spectroscopy (XPS), ¹³C solid-state nuclear magnetic resonance (NMR) spectroscopy, and Fourier-transform infrared (FT-IR) spectroscopy were performed on C1 Q_{SBA} , C8 Q_{SBA} , and C18 Q_{SBA} in a previous study³⁵. XPS confirmed that quaternary ammonium was well-crosslinked to the SBA surface (Fig. S2). The ¹³C NMR and FT-IR spectra also showed that the alkyl chains were well grafted, as intended (Figs. S3 and S4, respectively).

Table 1 lists the major chemical characteristics of CBZ. The octanol–water partitioning coefficient ($\log K_{ow}$) value of 2.25 indicates that CBZ is hydrophobic. The high pK_a (13.9) indicates that, in aqueous solutions, CBZ exists in an undissociated state at almost all pH.

Results and discussion

Adsorption kinetics. Fig. 2 shows the temporal trend for the adsorption of CBZ by Q_{SBA} . The adsorption process reached equilibrium within 120 min. Table 2 lists the parameters for the various kinetics models. The fitting quality as determined based on the coefficient of determination (R^2) was the best in the case of the pseudo-first-order model (Fig. S5). The equilibrium q_t (i.e., q_e) values for C1 Q_{SBA} , C8 Q_{SBA} , and C18 Q_{SBA} as calculated using the pseudo-first-order model were 0.618, 2.279, and 10.988 mg/g, respectively. Thus, the q_t value varied with the alkyl chain length of Q_{SBA} . CBZ adsorption was enhanced by increasing the alkyl chain length of Q_{SBA} . In a previous study, C8 Q_{SBA} showed an adsorption capacity as high as 593 mg/g for hydrophobic and dissociated DCF³⁶. In this study, the hydrophobic adsorption of CBZ by C18 Q_{SBA} was even greater, owing to the longer alkyl chain of the latter. Thus, it was confirmed that the adsorption of undissociated PPCP molecules can be significantly enhanced by using Q_{SBA} with a long alkyl chain.

The k_1 value was calculated based on the fitted pseudo-first-order model to characterize the adsorption of CBZ by Q_{SBA} . The k_1 value decreased with increasing alkyl chain length, with the values for C1 Q_{SBA} , C8 Q_{SBA} , and C18 Q_{SBA} , being 3.623, 0.327, and 0.198 L/min, respectively. The trends for q_e and k_1 were opposite because an increase in the alkyl chain of Q_{SBA} meant more adsorption sites and thus more time required to reach equilibrium.

Effect of initial CBZ concentration. Figure 3 shows the effect of the initial concentration of CBZ on its adsorption by Q_{SBA} . The observed data were analyzed using various isotherm models such as the Freundlich, Langmuir, and Redlich–Peterson models (Fig. S6). Table 3 lists the parameters of the isotherm models. Similar to the trend seen in the kinetics, the Q_{SBA} samples with longer alkyl chains exhibited higher maximum adsorption

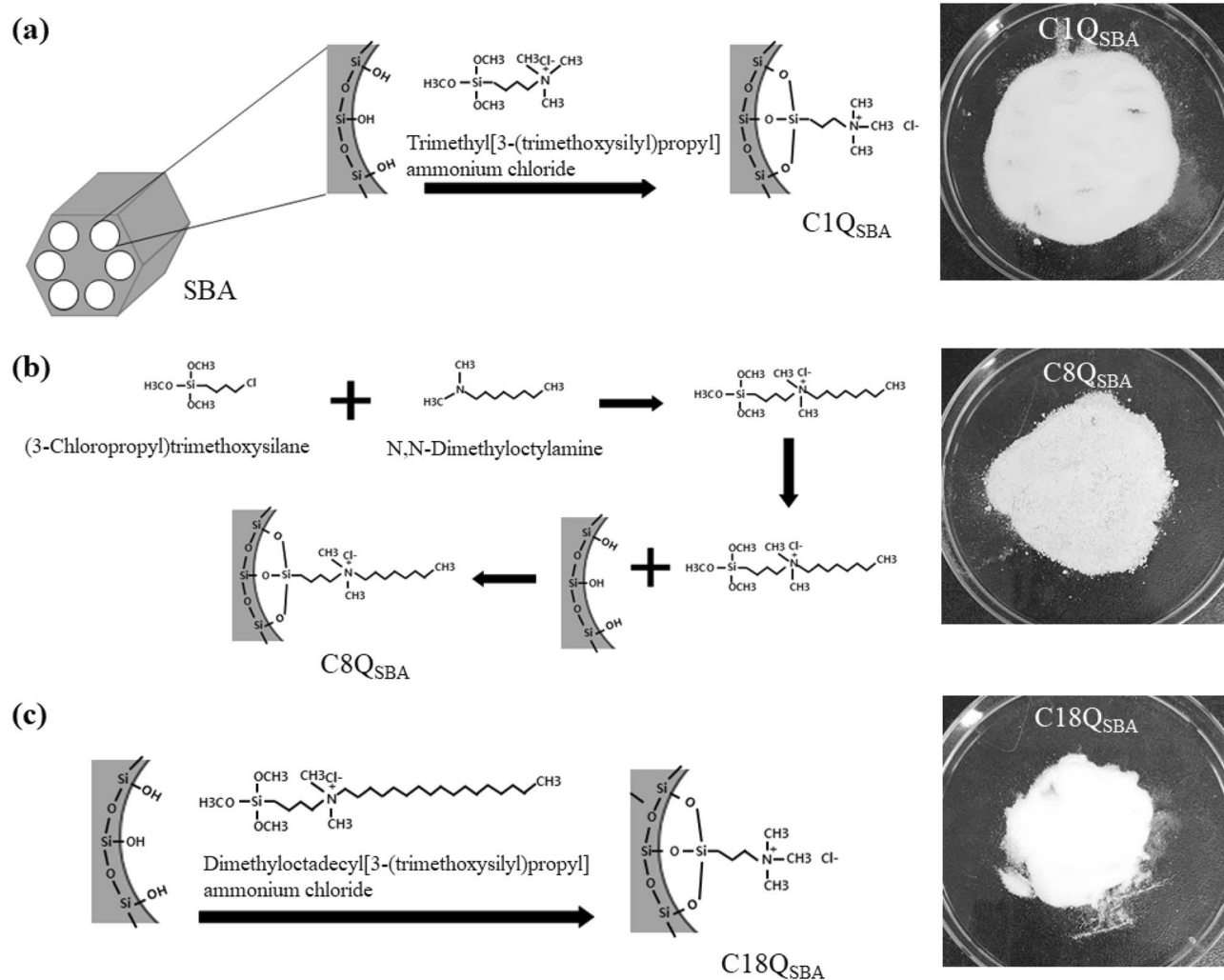


Figure 1. Schematics of the procedures for preparing Q_{SBA} samples and their digital images: (a) $C1Q_{SBA}$, (b) $C8Q_{SBA}$, and (c) $C18Q_{SBA}$. Figure was modified from Kang and Kim³⁵.

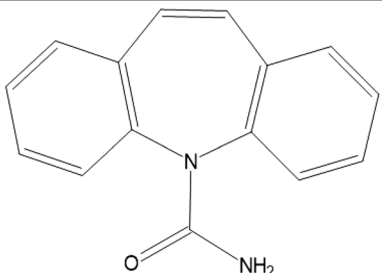
Name	Chemical structure	Molecular weight	$\log K_{ow}$	pK_a	Intrinsic solubility (S_0)	Wavelength for measurement
Carbamazepine (CBZ)		236.27	2.45 ⁴⁰	13.9 ⁴¹	112–236 mg/L ¹⁹	285 nm ⁴⁹

Table 1. Characteristics of CBZ.

capacities (Q_m) in the case of the Langmuir model (3.14, 6.56, and 24.5 mg/g for $C1Q_{SBA}$, $C8Q_{SBA}$, and $C18Q_{SBA}$, respectively). As mentioned previously, the adsorption capacities of $C8Q_{SBA}$ and $C18Q_{SBA}$ were higher because of favorable hydrophobic interactions.

Regardless of the length of the alkyl chain, the Redlich–Peterson model was the most suitable of the three isotherm models used, based on their SSE and R^2 values (Table 3). All three models showed high R^2 values (>0.967), which were acceptable for model fitting. This was probably because the experiments were not performed using high CBZ concentrations. The Langmuir model assumes monolayer adsorption, while the Freundlich model

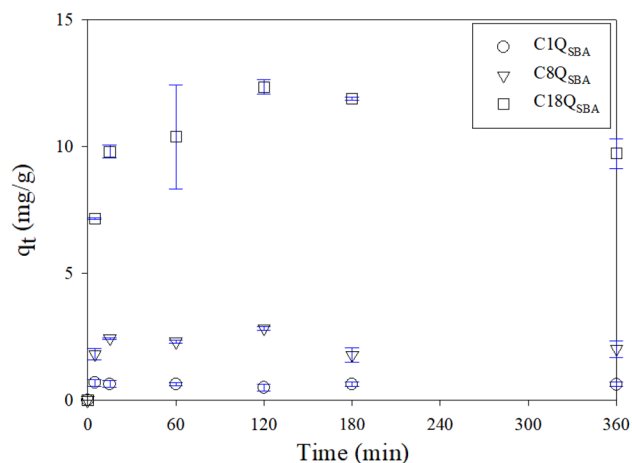


Figure 2. Effect of contact time on adsorption of CBZ by Q_{SBA} .

Q_{SBA}	Kinetics models											
	Pseudo-first-order				Pseudo-second-order				Elovich			
	q_e (mg/g)	k_1 (1/min)	SSE (mg^2/g^2)	R^2 (-)	q_e (mg/g)	k_2 (g/mg/min)	SSE (mg^2/g^2)	R^2 (-)	α (mg/g/min)	β (g/mg)	SSE (mg^2/g^2)	R^2 (-)
C1 Q_{SBA}	0.618	3.623	0.0203	0.942	0.618	2440	0.0203	0.942	2.29×10^{59}	236	0.0227	0.935
C8 Q_{SBA}	2.279	0.327	0.648	0.870	2.199	113	0.821	0.835	1.00×10^{24}	28.5	0.817	0.836
C18 Q_{SBA}	10.988	0.198	5.051	0.953	11.4	0.0316	4.72	0.956	3.77×10^3	1.22	8.46	0.921

Table 2. Kinetics model parameters for adsorption of CBZ by Q_{SBA} .

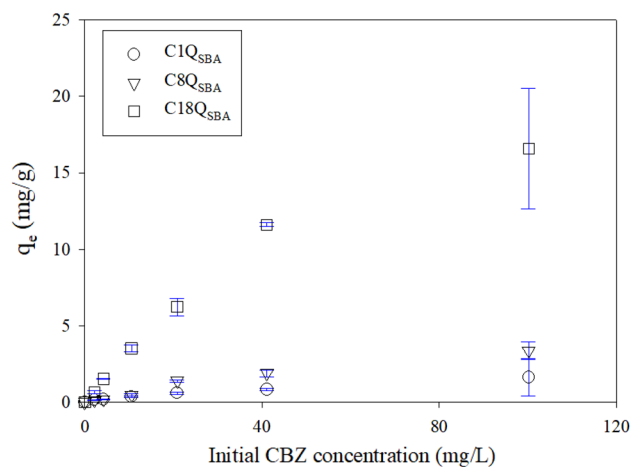


Figure 3. Effect of initial concentration of CBZ on its adsorption by Q_{SBA} .

Q_{SBA}	Equilibrium models												
	Freundlich				Langmuir				Redlich–Peterson				
	K_F (L/g)	$1/n$ (-)	SSE (mg^2/g^2)	R^2 (-)	Q_m (mg/g)	K_L (L/mg)	SSE (mg^2/g^2)	R^2 (-)	K_R (L/g)	a_R (1/mg)	g (-)	SSE (mg^2/g^2)	R^2 (-)
C1 Q_{SBA}	0.0734	0.672	0.00461	0.997	3.14	0.0104	0.0240	0.984	12.6	170	0.331	0.00463	0.997
C8 Q_{SBA}	0.135	0.709	0.184	0.977	6.56	0.0110	0.104	0.987	0.0720	0.0110	1.00	0.104	0.987
C18 Q_{SBA}	1.33	0.580	7.23	0.963	24.5	0.0263	1.36	0.993	0.644	0.0263	1.00	1.36	0.993

Table 3. Equilibrium model parameters for CBZ adsorption by Q_{SBA} .

assumes multilayer adsorption³². However, both the Freundlich and Langmuir models showed linear adsorption characteristics within a certain early concentration range. Detailed characterization of the adsorption models, such as considering single and multiple layers, is not possible owing to the limited solubility of CBZ. Thus, the standard Langmuir model is a suitable one because Q_{SBA} would have a larger surface available for adsorption compared with that of CBZ. The adsorption characteristics of a number of PPCPs with limited solubility have been described previously using the Langmuir model, including CBZ^{20–52}, ibuprofen²⁹, levofloxacin⁵³, sulfamethoxazole^{54–56}, tylosin⁵⁵, and 17 β -estradiol⁵⁶.

Table S3 compares the adsorption capacities of the various adsorbents for CBZ. Most adsorbents are based on activated carbon, mesoporous silica, or metal–organic frameworks. The data in Table S3 suggest that the primary mechanism for the adsorption of CBZ is hydrophobic interactions^{16–20}. Deng et al.¹⁹ and Jun et al.²⁰ reported Q_m values of 104.17 and 250.4 mg/g for CBZ using carbon-dot-modified magnetic carbon nanotubes and a metal–organic framework (Basolite A100), respectively. These values are much larger than that of C18 Q_{SBA} (24.5 mg/g). However, no study has attempted to control the hydrophobicity of the adsorbent to confirm that hydrophobic interactions are indeed the adsorption mechanism responsible for the removal of CBZ. In this study, we show clearly that the removal of CBZ is improved owing to the higher hydrophobicity owing to the longer alkyl chains. We also analyzed the effects of the pH and ionic strength to confirm that the enhancement in the hydrophobic interactions is not affected by the various wastewater characteristics.

Effect of initial pH. In a previous study, the adsorption of DCF onto C8 Q_{SBA} was reduced after an increase in the initial pH from 5 to 12. This suggests that DCF adsorption onto C8 Q_{SBA} involves not only hydrophobic interactions but also an anion exchange with the N^+ moiety of the quaternary ammonium group. Unlike CBZ, DCF dissociates into negatively charged molecules at $pH > 4.15$ ($pK_a = 4.15$)³⁵. Consequently, the pH controls both the hydrophobic and hydrophilic interactions and determines the adsorption efficiency of DCF by Q_{SBA} . Figure 4 shows the effect of the initial pH on CBZ removal by Q_{SBA} . Despite the variations in the initial pH, stable adsorption capacities were observed (0.41–0.92, 1.70–2.24, and 7.56–9.10 mg/g for C1 Q_{SBA} , C8 Q_{SBA} , and C18 Q_{SBA} , respectively); the exception was when the pH was 2 and C18 Q_{SBA} was used. Thus, the pH had a limited effect on the interactions between CBZ and Q_{SBA} . However, C18 Q_{SBA} showed an improved adsorption capacity of 12.06 ± 0.07 mg/g at pH 2. The pH of the CBZ solution was adjusted using HCl and NaOH. Thus, it was expected that an extremely low pH would improve the hydrophobic interactions at high concentrations of H^+ and Cl^- . The H^+ and Cl^- concentrations at pH 2 were 10 mM. It is known that when ions and proteins are present in high concentrations, they compete to interact with the water molecules, and unreacted proteins are precipitated by the hydrophobic interactions⁵⁷. Similarly, Bautista-Toledo et al.⁵⁸ explained that the enhancement in the adsorption of sodium dodecylbenzenesulfonate (SDBS) on activated carbon with increasing ionic strength was owing to the decreased solvation of SDBS because of the high ionic strength, which increased the hydrophobic-interaction-based adsorption. Likewise, the high concentrations of H^+ and Cl^- may have enhanced the hydrophobic interactions between C18 Q_{SBA} and CBZ in the present study. Similarly, the Na^+ and OH^- ions probably also aided the enhancement in the hydrophobic interactions when present in a high concentration at pH 10. However, the concentrations of Na^+ and OH^- were 0.1 mM at pH 10 and only 1/100th of those of H^+ and Cl^- at pH 2. The effect of the ion strength on the hydrophobic interactions between CBZ and Q_{SBA} was verified using NaCl, as described in the next section.

Effect of ionic strength. Figure 5 shows the effect of the ionic strength on the adsorption of CBZ by Q_{SBA} . The adsorption capacity increased with increasing ionic strength. The amounts of CBZ adsorbed were 0.70 ± 0.09 , 2.25 ± 0.14 , and 9.27 ± 0.42 mg/g for C1 Q_{SBA} , C8 Q_{SBA} , and C18 Q_{SBA} when 0.1 mM NaCl was used. In contrast, the adsorption capacities increased to 0.96 ± 0.33 , 2.77 ± 0.29 , and 14.94 ± 0.17 mg/g for C1 Q_{SBA} , C8 Q_{SBA} , and C18 Q_{SBA} , respectively, in the case of 100 mM NaCl. These values are 1.38, 1.23, and 1.61 times

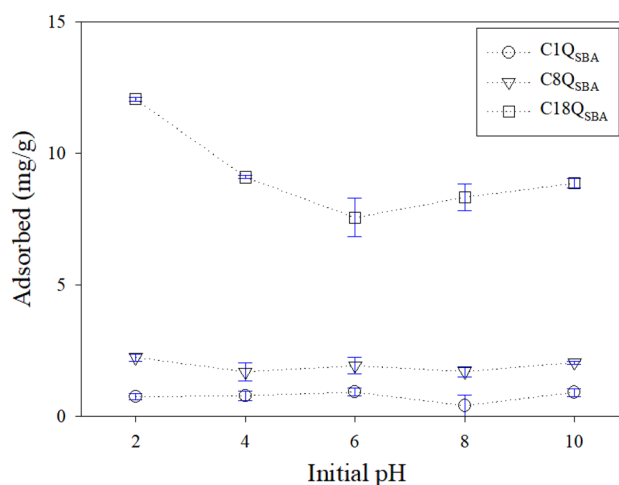


Figure 4. Effect of pH on CBZ adsorption by Q_{SBA} .

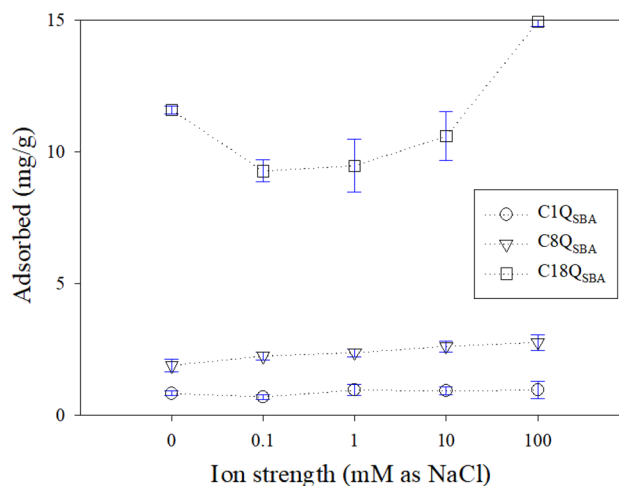


Figure 5. Effect of ionic strength on CBZ adsorption by Q_{SBA} .

higher, respectively, than the corresponding ones for 0.1 mM NaCl. The high salt concentration enhanced the hydrophobic interactions and shielded the electrostatic attraction between CBZ and the N^+ moiety of Q_{SBA} ^{32,59}. Interestingly, only in the case of $C18Q_{SBA}$ did the adsorption capacity exhibit high sensitivity to the ionic strength, with $C18Q_{SBA}$ showing an enhanced adsorption capacity of 10.60 ± 0.92 mg/g when 10 mM NaCl was used. The ionic concentrations in this case were similar to those at pH 2. Thus, it was confirmed that the hydrophobic interactions are predominantly controlled by the ionic strength and not the pH. The reason for the highest sensitivity of $C18Q_{SBA}$ was not clear. However, we believe that its longer alkyl chain exhibits stronger hydrophobic interactions in saline conditions. This means that the alkyl chain length can be increased to improve the efficiency of CBZ removal from wastewater samples with high ionic strength. The critical ionic strength of 100 mM NaCl (≈ 12 – 20 mS/cm^{60,61}) is higher than that of surface water (0.9 mS/cm), sanitary sewage (1.5–3.0 mS/cm), and treated water (0.22–0.37 mS/cm) but similar to that of industrial wastewater (35–70 mS/cm) and sea water (30 mS/cm)^{62–64}. This characteristic should allow for a high CBZ adsorption capacity in strongly ionic wastewaters. However, additional investigations are required to confirm the applicability of Q_{SBA} for use with wastewaters with high ionic strength.

Conclusions

Batch experiments were performed to investigate the primary mechanism of CBZ adsorption on Q_{SBA} with different alkyl chain lengths. The efficiency of CBZ adsorption by Q_{SBA} increased with increases in the reaction time and alkyl chain length of Q_{SBA} . Based on the Langmuir isotherm model, the maximum sorption capacities for $C1Q_{SBA}$, $C8Q_{SBA}$, and $C18Q_{SBA}$ were determined to be 3.14, 6.56, and 24.5 mg/g, respectively. Regarding the effect of the initial pH, the adsorption capacity was mostly stable within the pH range of 4–10; the exception was a pH of 2. Because the pK_a value of CBZ is 13.9, undissociated CBZ does not interact with the N^+ ions of Q_{SBA} . Consequently, it was assumed that hydrophobic interactions would be dominant in the pH range investigated in this study. The increase in CBZ adsorption at higher ionic strengths (similar to those of actual wastewater) is also attributable to the hydrophobic interactions between the alkyl chains of Q_{SBA} and CBZ. Thus, by controlling the alkyl chain length of Q_{SBA} , we were able to elucidate the CBZ adsorption mechanism in detail. Moreover, by comparing the adsorption characteristics of various PPCPs by adjusting the alkyl chain length of Q_{SBA} , it should not only be possible to determine the adsorption mechanism but also use the appropriate adsorbent for PPCPs based on their characteristics such as their hydrophobicity.

Data availability

The datasets used and/or analysed during the current study available from the corresponding author on reasonable request.

Received: 15 December 2022; Accepted: 21 March 2023

Published online: 30 March 2023

References

- Ali, I., Singh, P., Aboul-Enein, H. Y. & Sharma, B. Chiral analysis of ibuprofen residues in water and sediment. *Anal. Lett.* **42**, 1747–1760. <https://doi.org/10.1080/00032710903060768> (2009).
- Basheer, A. A. New generation nano-adsorbents for the removal of emerging contaminants in water. *J. Mol. Liq.* **261**, 583–593. <https://doi.org/10.1016/j.molliq.2018.04.021> (2018).
- Cheng, S., Xie, P., Yu, Z., Gu, R. & Wu, W. Hydroxyl-modified zirconia/porous carbon nanocomposite used as a highly efficient and renewable adsorbent for removal of carbamazepine from water. *Environ. Res.* **214**, 114030. <https://doi.org/10.1016/j.envres.2022.114030> (2022).
- Bai, Z. *et al.* Carbamazepine induces hepatotoxicity in zebrafish by inhibition of the Wnt/ β -catenin signaling pathway. *Environ. Pollut.* **276**, 116688. <https://doi.org/10.1016/j.envpol.2021.116688> (2021).

5. Wei, W. *et al.* The graceful art, significant function and wide application behavior of ultrasound research and understanding in carbamazepine (CBZ) enhanced removal and degradation by Fe₀/PDS/US. *Chemosphere* **278**, 130368. <https://doi.org/10.1016/j.chemosphere.2021.130368> (2021).
6. Mahlangu, T. O., Hoek, E. M. V., Mamba, B. B. & Verliefe, A. R. D. Influence of organic, colloidal and combined fouling on NF rejection of NaCl and carbamazepine: Role of solute–foulant–membrane interactions and cake-enhanced concentration polarisation. *J. Membr. Sci.* **471**, 35–46. <https://doi.org/10.1016/j.memsci.2014.07.065> (2014).
7. Vergili, I. Application of nanofiltration for the removal of carbamazepine, diclofenac and ibuprofen from drinking water sources. *J. Environ. Manag.* **127**, 177–187. <https://doi.org/10.1016/j.jenvman.2013.04.036> (2013).
8. Dwivedi, K., Morone, A., Chakrabarti, T. & Pandey, R. A. Evaluation and optimization of fenton pretreatment integrated with granulated activated carbon (GAC) filtration for carbamazepine removal from complex wastewater of pharmaceutical industry. *J. Environ. Chem. Eng.* **6**, 3681–3689. <https://doi.org/10.1016/j.jece.2016.12.054> (2018).
9. Laera, G., Chong, M. N., Jin, B. & Lopez, A. An integrated MBR–TiO₂ photocatalysis process for the removal of Carbamazepine from simulated pharmaceutical industrial effluent. *Bioresour. Technol.* **102**, 7012–7015. <https://doi.org/10.1016/j.biortech.2011.04.056> (2011).
10. Lee, S. *et al.* Evaluating controllability of pharmaceuticals and metabolites in biologically engineered processes, using corresponding octanol–water distribution coefficient. *Ecol. Eng.* **37**, 1595–1600. <https://doi.org/10.1016/j.ecoleng.2011.04.007> (2011).
11. Nguyen, H. T., Adil, S., Cho, K., Jeong, S. & Kim, E.-J. Improvement of carbamazepine removal through biodegradation coupled with peroxymonosulfate-based Fenton oxidation. *J. Environ. Chem. Eng.* **10**, 108150. <https://doi.org/10.1016/j.jece.2022.108150> (2022).
12. Souza-Chaves, B. M. D. *et al.* Advanced electrochemical oxidation applied to benzodiazepine and carbamazepine removal: Aqueous matrix effects and neurotoxicity assessments employing rat hippocampus neuronal activity. *J. Water Process. Eng.* **49**, 102990. <https://doi.org/10.1016/j.jwpe.2022.102990> (2022).
13. Wang, Y. *et al.* A novel peroxymonosulfate (PMS)-enhanced iron coagulation process for simultaneous removal of trace organic pollutants in water. *Water Res.* **185**, 116136. <https://doi.org/10.1016/j.watres.2020.116136> (2020).
14. Bogunović, M. *et al.* Removal of selected emerging micropollutants from wastewater treatment plant effluent by advanced non-oxidative treatment—A lab-scale case study from Serbia. *Sci. Total Environ.* **765**, 142764. <https://doi.org/10.1016/j.scitotenv.2020.142764> (2021).
15. Mondol, M. M. H., Yoo, D. K. & Jhung, S. H. Adsorptive removal of carbamazepine and ibuprofen from aqueous solution using a defective Zr-based metal-organic framework. *J. Environ. Chem. Eng.* **10**, 108560. <https://doi.org/10.1016/j.jece.2022.108560> (2022).
16. Suriyanon, N., Punyapalukul, P. & Ngamcharussrivichai, C. Mechanistic study of diclofenac and carbamazepine adsorption on functionalized silica-based porous materials. *Chem. Eng. J.* **214**, 208–218. <https://doi.org/10.1016/j.cej.2012.10.052> (2013).
17. He, Q. *et al.* Removal of the environmental pollutant carbamazepine using molecular imprinted adsorbents: Molecular simulation, adsorption properties, and mechanisms. *Water Res.* **168**, 115164. <https://doi.org/10.1016/j.watres.2019.115164> (2020).
18. Chen, C. *et al.* Adsorption behaviors of organic micropollutants on zirconium metal-organic framework UiO-66: Analysis of surface interactions. *ACS Appl. Mater. Interfaces* **9**, 41043–41054. <https://doi.org/10.1021/acsami.7b13443> (2017).
19. Deng, Y., Ok, Y. S., Mohan, D., Pittman, C. U. & Dou, X. Carbamazepine removal from water by carbon dot-modified magnetic carbon nanotubes. *Environ. Res.* **169**, 434–444. <https://doi.org/10.1016/j.envres.2018.11.035> (2019).
20. Jun, B.-M., Heo, J., Park, C. M. & Yoon, Y. Comprehensive evaluation of the removal mechanism of carbamazepine and ibuprofen by metal organic framework. *Chemosphere* **235**, 527–537. <https://doi.org/10.1016/j.chemosphere.2019.06.208> (2019).
21. Ali, I. *et al.* Advances in carbon nanomaterials as lubricants modifiers. *J. Mol. Liq.* **279**, 251–266. <https://doi.org/10.1016/j.molliq.2019.01.113> (2019).
22. Basheer, A. A. Advances in the smart materials applications in the aerospace industries. *Aircr. Eng. Aerosp. Technol.* **92**, 1027–1035. <https://doi.org/10.1108/aeat-02-2020-0040> (2020).
23. Burakova, I. V. *et al.* Kinetics of the adsorption of scandium and cerium ions in sulfuric acid solutions on a nanomodified activated carbon. *J. Mol. Liq.* **253**, 277–283. <https://doi.org/10.1016/j.molliq.2018.01.063> (2018).
24. Rajapaksha, A. U., Dilrukshi Premarathna, K. S., Gunarathne, V., Ahmed, A. & Vithanage, M. in *Pharmaceuticals and Personal Care Products: Waste Management and Treatment Technology* (eds. Majeti Narasimha Vara Prasad, Meththika Vithanage, & Atya Kapley) 213–238 (Butterworth-Heinemann, 2019).
25. Ali, I. *et al.* High-speed and high-capacity removal of methyl orange and malachite green in water using newly developed mesoporous carbon: Kinetic and isotherm studies. *ACS Omega* **4**, 19293–19306. <https://doi.org/10.1021/acso.9b02669> (2019).
26. Al-Shaalan, N. H., Ali, I., Allothman, Z. A., Al-Wahaibi, L. H. & Alabdulmonem, H. High performance removal and simulation studies of diuron pesticide in water on MWCNTs. *J. Mol. Liq.* **289**, 111039. <https://doi.org/10.1016/j.molliq.2019.111039> (2019).
27. Wang, T. *et al.* Adsorptive removal of PPCPs from aqueous solution using carbon-based composites: A review. *Chin. Chem. Lett.* <https://doi.org/10.1016/j.ccl.2021.09.029> (2021).
28. Zhu, X. *et al.* Insights into the adsorption of pharmaceuticals and personal care products (PPCPs) on biochar and activated carbon with the aid of machine learning. *J. Hazard. Mater.* **423**, 127060. <https://doi.org/10.1016/j.jhazmat.2021.127060> (2022).
29. Zhu, Z., Xie, J., Zhang, M., Zhou, Q. & Liu, F. Insight into the adsorption of PPCPs by porous adsorbents: Effect of the properties of adsorbents and adsorbates. *Environ. Pollut.* **214**, 524–531. <https://doi.org/10.1016/j.envpol.2016.04.070> (2016).
30. Teixidó, M., Pignatello, J. J., Beltrán, J. L., Granados, M. & Peccia, J. Speciation of the ionizable antibiotic sulfamethazine on black carbon (Biochar). *Environ. Sci. Technol.* **45**, 10020–10027. <https://doi.org/10.1021/es202487h> (2011).
31. Yoon, Y., Westerhoff, P., Snyder, S. A. & Esparza, M. HPLC-fluorescence detection and adsorption of bisphenol A, 17 β -estradiol, and 17 α -ethynyl estradiol on powdered activated carbon. *Water Res.* **37**, 3530–3537. [https://doi.org/10.1016/S0043-1354\(03\)00239-2](https://doi.org/10.1016/S0043-1354(03)00239-2) (2003).
32. Chen, W.-Y., Liu, Z.-C., Lin, P.-H., Fang, C.-I. & Yamamoto, S. The hydrophobic interactions of the ion-exchanger resin ligands with proteins at high salt concentrations by adsorption isotherms and isothermal titration calorimetry. *Sep. Purif. Technol.* **54**, 212–219. <https://doi.org/10.1016/j.seppur.2006.09.008> (2007).
33. Celiz, M. D., Pérez, S., Barceló, D. & Aga, D. S. Trace analysis of polar pharmaceuticals in wastewater by LC–MS–MS: Comparison of membrane bioreactor and activated sludge systems. *J. Chromatogr. Sci.* **47**, 19–25. <https://doi.org/10.1093/chromsci/47.1.19> (2009).
34. Kosjek, T., Andersen, H. R., Kompare, B., Ledin, A. & Heath, E. Fate of carbamazepine during water treatment. *Environ. Sci. Technol.* **43**, 6256–6261. <https://doi.org/10.1021/es900070h> (2009).
35. Kang, J.-K. & Kim, S.-B. Synthesis of quaternized mesoporous silica SBA-15 with different alkyl chain lengths for selective nitrate removal from aqueous solutions. *Microporous Mesoporous Mater.* **295**, 109967. <https://doi.org/10.1016/j.micromeso.2019.109967> (2020).
36. Kang, J.-K. *et al.* Artificial neural network and response surface methodology modeling for diclofenac removal by quaternized mesoporous silica SBA-15 in aqueous solutions. *Microporous Mesoporous Mater.* **328**, 111497. <https://doi.org/10.1016/j.micromeso.2021.111497> (2021).
37. Jin, J. *et al.* Novel magnetic carboxyl modified hypercrosslinked resins for effective removal of typical PPCPs. *Chemosphere* **185**, 563–573. <https://doi.org/10.1016/j.chemosphere.2017.07.058> (2017).
38. Wei, X. *et al.* Adsorption of pharmaceuticals and personal care products by deep eutectic solvents-regulated magnetic metal-organic framework adsorbents: Performance and mechanism. *Chem. Eng. J.* **392**, 124808. <https://doi.org/10.1016/j.cej.2020.124808> (2020).

39. Llinàs, A., Burley, J. C., Box, K. J., Glen, R. C. & Goodman, J. M. Diclofenac solubility: Independent determination of the intrinsic solubility of three crystal forms. *J. Med. Chem.* **50**, 979–983. <https://doi.org/10.1021/jm0612970> (2007).
40. Dal Pozzo, A., Donzelli, G., Rodriguez, L. & Tajana, A. “In vitro” model for the evaluation of drug distribution and plasma protein-binding relationships. *Int. J. Pharm.* **50**, 97–101. [https://doi.org/10.1016/0378-5173\(89\)90133-6](https://doi.org/10.1016/0378-5173(89)90133-6) (1989).
41. Jones, O. A., Voulvoulis, N. & Lester, J. N. Aquatic environmental assessment of the top 25 English prescription pharmaceuticals. *Water Res.* **36**, 5013–5022. [https://doi.org/10.1016/s0043-1354\(02\)00227-0](https://doi.org/10.1016/s0043-1354(02)00227-0) (2002).
42. Morissette, M. F., Vo Duy, S., Arp, H. P. H. & Sauvé, S. Sorption and desorption of diverse contaminants of varying polarity in wastewater sludge with and without alum. *Environ. Sci. Process. Impacts* **17**, 674–682. <https://doi.org/10.1039/C4EM00620H> (2015).
43. Lagergren, S. K. About the theory of so-called adsorption of soluble substances. *Sven. Vetenskapsakad. Handlingar* **24**, 1–39 (1898).
44. Ho, Y.-S. Review of second-order models for adsorption systems. *J. Hazard. Mater.* **136**, 681–689. <https://doi.org/10.1016/j.jhazmat.2005.12.043> (2006).
45. Roginsky, S. & Zeldovich, Y. B. The catalytic oxidation of carbon monoxide on manganese dioxide. *Acta Phys. Chem. USSR* **1**, 2019 (1934).
46. Freundlich, H. Über die adsorption in Lösungen. *Z. Phys. Chem.* **57U**, 385–470. <https://doi.org/10.1515/zpch-1907-5723> (1907).
47. Langmuir, I. The constitution and fundamental properties of solids and liquids. Part I. solids. *J. Am. Chem. Soc.* **38**, 2221–2295. <https://doi.org/10.1021/ja02268a002> (1916).
48. Jossens, L., Prausnitz, J. M., Fritz, W., Schlünder, E. U. & Myers, A. L. Thermodynamics of multi-solute adsorption from dilute aqueous solutions. *Chem. Eng. Sci.* **33**, 1097–1106. [https://doi.org/10.1016/0009-2509\(78\)85015-5](https://doi.org/10.1016/0009-2509(78)85015-5) (1978).
49. Rajendran, K. & Sen, S. Adsorptive removal of carbamazepine using biosynthesized hematite nanoparticles. *Environ. Nanotechnol. Monit. Manag.* **9**, 122–127. <https://doi.org/10.1016/j.enmm.2018.01.001> (2018).
50. Nezhadali, A., Koushali, S. E. & Divsar, F. Synthesis of polypyrrole–chitosan magnetic nanocomposite for the removal of carbamazepine from wastewater: Adsorption isotherm and kinetic study. *J. Environ. Chem. Eng.* **9**, 105648. <https://doi.org/10.1016/j.jece.2021.105648> (2021).
51. Lerman, I., Chen, Y., Xing, B. & Chefetz, B. Adsorption of carbamazepine by carbon nanotubes: Effects of DOM introduction and competition with phenanthrene and bisphenol A. *Environ. Pollut.* **182**, 169–176. <https://doi.org/10.1016/j.envpol.2013.07.010> (2013).
52. Bakkaloglu, S., Ersan, M., Karanfil, T. & Apul, O. G. Effect of superfine pulverization of powdered activated carbon on adsorption of carbamazepine in natural source waters. *Sci. Total Environ.* **793**, 148473. <https://doi.org/10.1016/j.scitotenv.2021.148473> (2021).
53. Xiang, Y. *et al.* A sustainable ferromanganese biochar adsorbent for effective levofloxacin removal from aqueous medium. *Chemosphere* **237**, 124464. <https://doi.org/10.1016/j.chemosphere.2019.124464> (2019).
54. Ninwiwek, N., Hongsawat, P., Punyapalukul, P. & Prarat, P. Removal of the antibiotic sulfamethoxazole from environmental water by mesoporous silica-magnetic graphene oxide nanocomposite technology: Adsorption characteristics, coadsorption and uptake mechanism. *Colloids Surf. A* **580**, 123716. <https://doi.org/10.1016/j.colsurfa.2019.123716> (2019).
55. Li, Z., Li, M., Che, Q., Li, Y. & Liu, X. Synergistic removal of tylosin/sulfamethoxazole and copper by nano-hydroxyapatite modified biochar. *Bioresour. Technol.* **294**, 122163. <https://doi.org/10.1016/j.biortech.2019.122163> (2019).
56. Wang, F., Sun, W., Pan, W. & Xu, N. Adsorption of sulfamethoxazole and 17 β -estradiol by carbon nanotubes/CoFe₂O₄ composites. *Chem. Eng. J.* **274**, 17–29. <https://doi.org/10.1016/j.cej.2015.03.113> (2015).
57. Novák, P. & Havlíček, V. in *Proteomic Profiling and Analytical Chemistry (Second Edition)* (eds P. Ciborowski & J. Silberring) 51–62 (Elsevier, 2016).
58. Bautista-Toledo, M. I., Méndez-Díaz, J. D., Sánchez-Polo, M., Rivera-Utrilla, J. & Ferro-García, M. A. Adsorption of sodium dodecylbenzenesulfonate on activated carbons: Effects of solution chemistry and presence of bacteria. *J. Colloid Interface Sci.* **317**, 11–17. <https://doi.org/10.1016/j.jcis.2007.09.039> (2008).
59. Hu, Y. *et al.* Dye adsorption by resins: Effect of ionic strength on hydrophobic and electrostatic interactions. *Chem. Eng. J.* **228**, 392–397. <https://doi.org/10.1016/j.cej.2013.04.116> (2013).
60. Daoudi, J., Betelu, S., Tzedakis, T., Bertrand, J. & Ignatiadis, I. A multi-parametric device with innovative solid electrodes for long-term monitoring of pH, redox-potential and conductivity in a nuclear waste repository. *Sensors* **17**, 1372. <https://doi.org/10.3390/s17061372> (2017).
61. Widodo, C. S., Sela, H. & Santosa, D. R. The effect of NaCl concentration on the ionic NaCl solutions electrical impedance value using electrochemical impedance spectroscopy methods. *AIP Conf. Proc.* **2021**, 050003. <https://doi.org/10.1063/1.5062753> (2018).
62. Lahav, O. & Birnhack, L. in *Aquatic Chemistry: For Water and Wastewater Treatment Applications*. (De Gruyter, 2019).
63. Zheng, Z. *et al.* Three-stage vertical distribution of seawater conductivity. *Sci. Rep.* **8**, 9916. <https://doi.org/10.1038/s41598-018-27931-y> (2018).
64. Salmerón, I., Oller, I. & Malato, S. Electro-oxidation process assisted by solar energy for the treatment of wastewater with high salinity. *Sci. Total Environ.* **705**, 135831. <https://doi.org/10.1016/j.scitotenv.2019.135831> (2020).

Acknowledgements

This work was supported by the National Research Foundation of Korea (NRF) grant funded by the Korea government (MSIT) (No. 2021R1C1C1009214). This research was also supported by Basic Science Research Program through the National Research Foundation of Korea (NRF) funded by the Ministry of Education (NRF-2021R1A6A1A03039572 AND NRF-2021R1I1A1A01057371).

Author contributions

J.-K.K.: Conceptualization, Performing experiments, Writing-original draft; H.L.: Performing experiments, Writing-original draft; S.-B.K.: Reviewing and editing; H.B.: Reviewing and editing, Supervision, Funding acquisition.

Competing interests

The authors declare that they have no known competing financial interests or personal relationships that could have appeared to influence the work reported in this paper.

Additional information

Supplementary Information The online version contains supplementary material available at <https://doi.org/10.1038/s41598-023-32108-3>.

Correspondence and requests for materials should be addressed to H.B.

Reprints and permissions information is available at www.nature.com/reprints.

Publisher's note Springer Nature remains neutral with regard to jurisdictional claims in published maps and institutional affiliations.



Open Access This article is licensed under a Creative Commons Attribution 4.0 International License, which permits use, sharing, adaptation, distribution and reproduction in any medium or format, as long as you give appropriate credit to the original author(s) and the source, provide a link to the Creative Commons licence, and indicate if changes were made. The images or other third party material in this article are included in the article's Creative Commons licence, unless indicated otherwise in a credit line to the material. If material is not included in the article's Creative Commons licence and your intended use is not permitted by statutory regulation or exceeds the permitted use, you will need to obtain permission directly from the copyright holder. To view a copy of this licence, visit <http://creativecommons.org/licenses/by/4.0/>.

© The Author(s) 2023